NANO LETTERS

pubs.acs.org/NanoLett

Letter

Charge Transfer Dynamics in $MoSe_2$/hBN/WSe_2 Heterostructures

Yoseob Yoon,* Zuocheng Zhang, Ruishi Qi, Andrew Y. Joe, Renee Sailus, Kenji Watanabe, Takashi Taniguchi, Sefaattin Tongay, and Feng Wang

Cite This: *Nano Lett.* 2022, 22, 10140−10146

Read Online

ACCESS | Metrics & More | Article Recommendations | Supporting Information

ABSTRACT: Ultrafast charge transfer processes provide a facile way to create interlayer excitons in directly contacted transition metal dichalcogenide (TMD) layers. More sophisticated heterostructures composed of TMD/hBN/TMD enable new ways to control interlayer exciton properties and achieve novel exciton phenomena, such as exciton insulators and condensates, where longer lifetimes are desired. In this work, we experimentally study the charge transfer dynamics in a heterostructure composed of a 1 nm thick hBN spacer between $MoSe_2$ and WSe_2 monolayers. We observe the hole transfer from $MoSe_2$ to WSe_2 through the hBN barrier with a time constant of 500 ps, which is over 3 orders of magnitude slower than that between TMD layers without a spacer. Furthermore, we observe strong competition between the interlayer charge transfer and intralayer exciton−exciton annihilation processes at high excitation densities. Our work opens possibilities to understand charge transfer pathways in TMD/hBN/TMD heterostructures for the efficient generation and control of interlayer excitons.

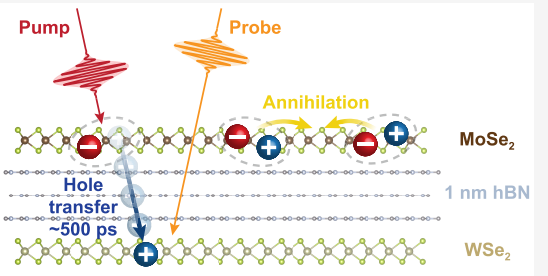

KEYWORDS: *Ultrafast dynamics, transient absorption spectroscopy, interlayer charge transfer, exciton−exciton annihilation, van der Waals heterostructures*

Interlayer excitons are bound electron−hole pairs where the constituent electron and hole are spatially separated near the junction of two layered semiconductors. They are energetically favorable in a heterobilayer with type-II band alignment or in a homobilayer with an out-of-plane electric field. In directly contacted transition metal dichalcogenide (TMD) heterostructures, interlayer excitons can be easily generated by any optical excitations above one of the intralayer exciton energies, owing to ultrafast and efficient charge transfer processes from one layer to the other.[1−4]

Adding a thin hexagonal boron nitride (hBN) layer to make a TMD/hBN/TMD heterostructure provides the opportunity to engineer many properties of the interlayer excitons, such as their binding energy, dipolar exciton−exciton interaction strength, and charge transfer dynamics. Since electrons reside in one layer and holes reside in the other layer that are separated by the hBN layer, the spatial overlap between their wave functions is poor, and their radiative lifetimes can be much longer[5] than those of directly contacted TMD/TMD heterostructures.[6−9] A long lifetime is one of the key properties that allows us to reach novel excitonic phases in equilibrium, including excitonic insulators[5,10,11] and Bose−Einstein condensates,[12] where excitons need to interact for a sufficiently long time before they recombine and disappear. In addition, the aligned nature of the permanent dipole moments of interlayer excitons leads to enhanced exciton−exciton interaction strength with increased hBN thickness.[13] The dipolar interaction strength of interlayer excitons can exceed the exchange interaction between neutral excitons, which can be used to stabilize strongly correlated excitonic phases.[5,14,15]

Although the hBN layer is beneficial for realizing long-lived and strongly correlated interlayer excitons, it exponentially suppresses the tunneling probability and the charge transfer rate. This will hamper the generation of such interlayer excitons through optical excitations. An experimental study of these effects in TMD/hBN/TMD heterostructures would be crucial for understanding the dynamics of interlayer exciton formation and for optimizing the strongly correlated excitonic phases.

Transient absorption spectroscopy is a powerful tool to investigate the interlayer exciton dynamics, where pump-induced changes of absorption peaks are probed as a function of the time delay between pump and probe pulses. Since the intralayer exciton peak changes (induced by the presence of interlayer excitons) are probed in these measurements, the vanishing oscillator strength of interlayer excitons[7] does not prohibit the measurement; for this reason, transient absorption spectroscopy has been primarily used to study the dynamics of

Received: October 13, 2022
Revised: December 3, 2022
Published: December 9, 2022

https://doi.org/10.1021/acs.nanolett.2c04030
Nano Lett. 2022, 22, 10140−10146

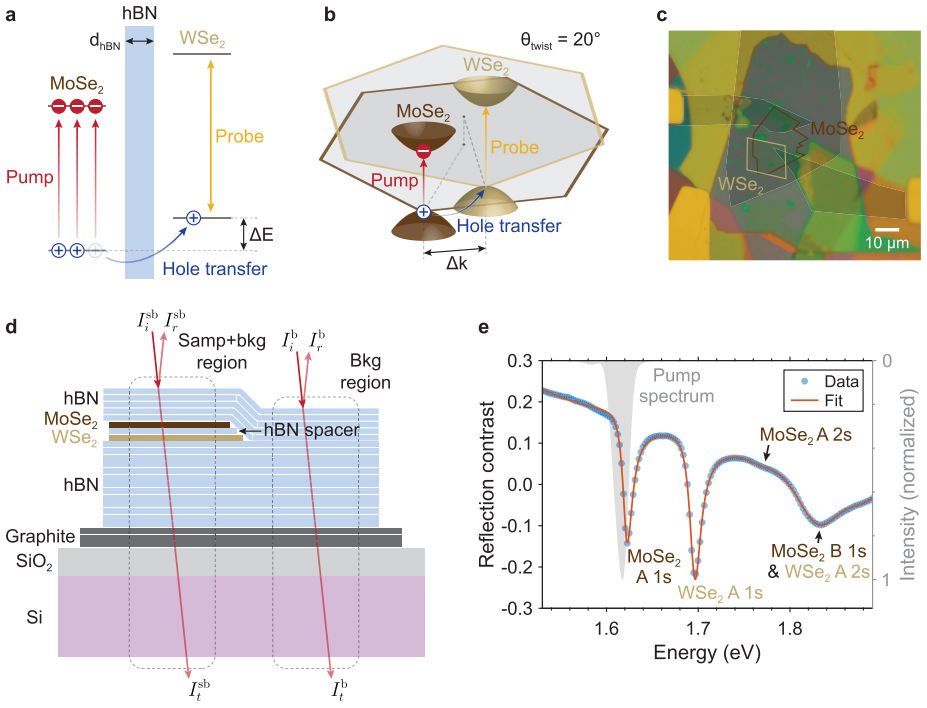

Figure 1. Charge transfer pathway and pump−probe measurement scheme. (a) Charge transfer pathway in real space. A quasiresonant pump pulse creates $MoSe_2$ excitons (red arrows). Holes in the $MoSe_2$ layer are transferred to the WSe_2 layer (blue arrow). The WSe_2 exciton absorption spectrum is monitored by a broadband probe pulse (yellow arrow). The transfer process is accompanied by a real-space displacement of holes by 1.6 nm (d_{hBN} = 1.0 nm) and energy relaxation by $\Delta E \approx 0.3$ eV. (b) Charge transfer pathway in momentum space. For the device with θ_{twist} = 20°, the transfer process is accompanied by a momentum shift of $\Delta k \approx 0.44$ Å^{-1}. (c) A microscope image of the $MoSe_2$/hBN/WSe_2 heterostructure. Graphite gates and contacts (gray shaded area) are grounded unless otherwise noted. (d) Schematic of the layered structure. Incident pulse intensity I_i is reflected (I_r), transmitted (I_t), and absorbed by the TMD layers, while only the reflected part is measured in the sample + background ("sb") region and the background ("b") region. (e) Reflection contrast spectrum at 100 K (blue circles) and a fit (orange line) using the transfer-matrix simulation described in the main text. A normalized pump spectrum is shown as the gray shaded area (inverted vertical axis on the right-hand side).

charge transfer processes.[1,16−22] Here, using the same technique, we investigate the ultrafast charge transfer dynamics in a heterostructure composed of a 1 nm thick hBN spacer between $MoSe_2$ and WSe_2 monolayers. We reveal that the hole transfer from $MoSe_2$ to WSe_2 across hBN takes place with a time constant of ∼500 ps, which is over 3 orders of magnitude slower than the charge transfer between directly contacted TMD layers (<100 fs). In addition, we show that there is a strong competition between the interlayer charge transfer and intralayer exciton−exciton annihilation processes in this system at high excitation densities.

Figure 1a,b illustrates our experimental scheme. We first create $MoSe_2$ intralayer excitons using a quasiresonant pump pulse, which essentially does not create WSe_2 excitons ($E_{pump} \approx E_{MoSe_2} < E_{WSe_2}$). After a time delay ($\Delta t = t_{probe} - t_{pump}$), a broadband probe pulse (1.55−1.91 eV) measures the WSe_2 intralayer exciton absorption peak. Holes dissociated from the $MoSe_2$ excitons are transferred to the WSe_2 layer and relaxed to its band edge, which saturate the WSe_2 intralayer exciton absorption by Pauli blocking. A microscope image and schematic layered structure are shown in Figure 1c,d, respectively. The hBN spacer consists of three atomic layers, which is confirmed by an atomic force microscope (AFM) measurement (see Figure S1a,b). The twist angle between $MoSe_2$ and WSe_2 layers is determined to be 19.5° by a polarization-dependent second-harmonic generation measurement (see Figure S1c).

Due to limitations in typical experimental configurations (e.g., opaque substrate or cryostat sample holder, see Figure S2), it is common that only the reflection is measured. To separate the optical features of the sample ($MoSe_2$/hBN/WSe_2) from the background (SiO_2/Si substrate and other dielectric layers) and to eliminate the effect of the uneven probe spectrum, we measure a reflection contrast spectrum, defined as $(I_r^{sb} - I_r^b)/I_r^b$, where I_r^{sb} is a reflection spectrum measured in a region with sample and background ("sb"), and I_r^b is a reflection spectrum measured in a background ("b") region, as defined in Figure 1d. The measured reflection contrast and pump spectra are shown in Figure 1e. The pump is mostly resonant with $MoSe_2$ excitons, although it is slightly red-shifted to reduce the direct generation of WSe_2 excitons and carriers. The small spectral mismatch is taken into account in the calibration of pump absorption by the $MoSe_2$ layer (see Figure S4).

The local field at the TMD layers can be vastly different from that of a free-space field due to the interference between reflections from multiple interfaces in the layered structure. Depending on the structure's dimensions and dielectric properties, the Fano-like line shapes and peak heights of resonances can dramatically vary even with the same TMD layer. Therefore, it is crucial to perform transfer-matrix calculations to estimate the absolute values of absorption (see the Supporting Information for details of the calibration). A result of the transfer-matrix fitting to the measured reflection contrast spectrum, starting from known thicknesses and

https://doi.org/10.1021/acs.nanolett.2c04030
Nano Lett. 2022, 22, 10140−10146

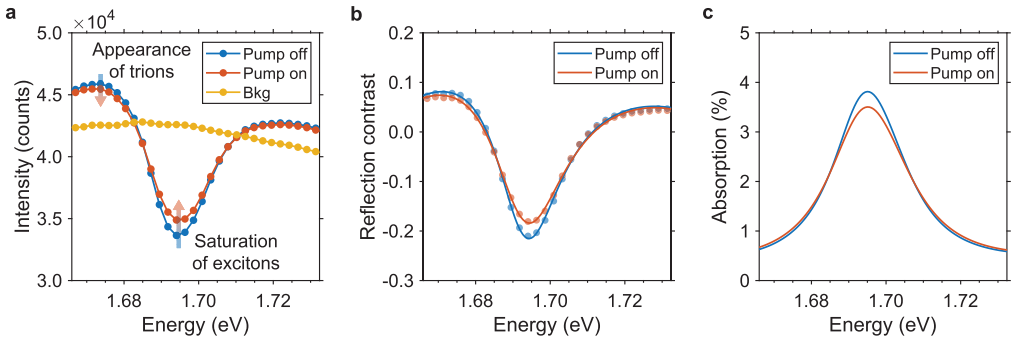

Figure 2. Determination of WSe_2 absorption spectra with and without the pump at 100 K. (a) Raw reflection intensities of the broadband probe in the background region (yellow), in the sample region without the pump (blue), and in the sample region with the pump (orange). The pump fluence was $F_{pump} = 39.4\ \mu J/cm^2$, corresponding to the initial $MoSe_2$ exciton density $n_m(\Delta t = 0) = 3.0 \times 10^{12}\ cm^{-2}$. The pump-on spectrum is taken at a time delay of 30 ps, when the hole transfer process is completed. (b) Reflection contrast spectra with and without the pump (blue and orange circles, respectively). The best fits to the transfer-matrix calculations are shown as blue and orange lines. (c) Extracted absorption profiles with and without the pump (blue and orange lines, respectively).

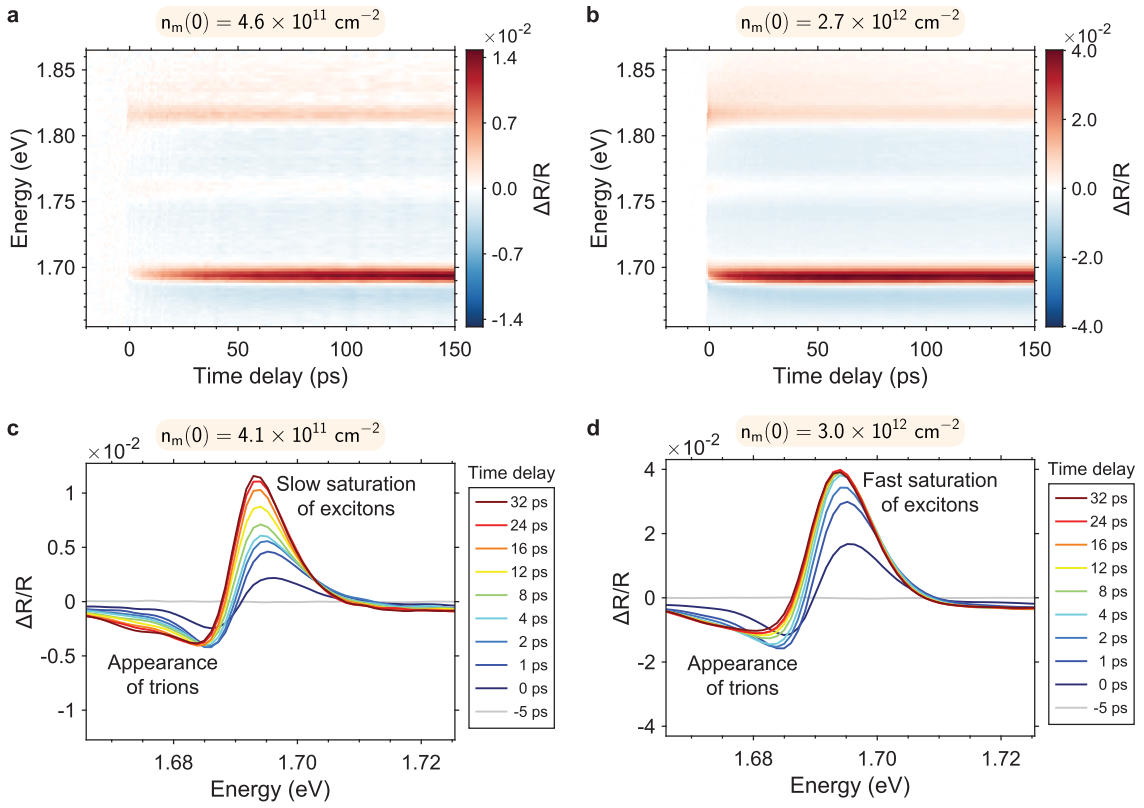

Figure 3. Pump−probe spectra at 100 K and transient spectral analysis. (a,b) Differential transient reflection spectra ($\Delta R/R$) as a function of the probe energy and time delay at low and high pump fluences. (c,d) Line cuts of transient reflection spectra at various time delays (different colors) and at low and high pump fluences.

dielectric constants of each layer, is shown as the orange line in Figure 1e. From the absolute values of the reflection contrast spectrum, not only are the central energies and line widths extracted but also the absolute values of absorption by each TMD layer are determined (see Figure S4), which cannot be simply read from the reflection contrast values.

Figure 2a shows representative transient reflection spectra measured by the probe with and without the pump, which we denote as $R_{pump\ on}$ and $R_{pump\ off}$, respectively. The pump-on spectrum is taken with a high pump fluence ($F_{pump} = 39.4\ \mu J/cm^2$) and at a pump−probe time delay when the hole transfer is completed ($\Delta t = 30$ ps). A probe spectrum in the background region is also measured to obtain the reflection contrast spectra shown in Figure 2b. At this high pump fluence, the exciton absorption peak saturates, and the trion absorption peak (~20 meV below the exciton energy) emerges. Transfer-matrix calculations including these two peaks can successfully reproduce the measured reflection contrast spectra shown in Figure 2b, and the extracted absorption profiles are shown in Figure 2c.

We then varied the time delay to measure the charge transfer dynamics. Figure 3a,b shows the transient reflection spectra at low and high pump fluences, respectively. To visualize small changes in the reflection intensities, we plotted their

https://doi.org/10.1021/acs.nanolett.2c04030
Nano Lett. 2022, 22, 10140−10146

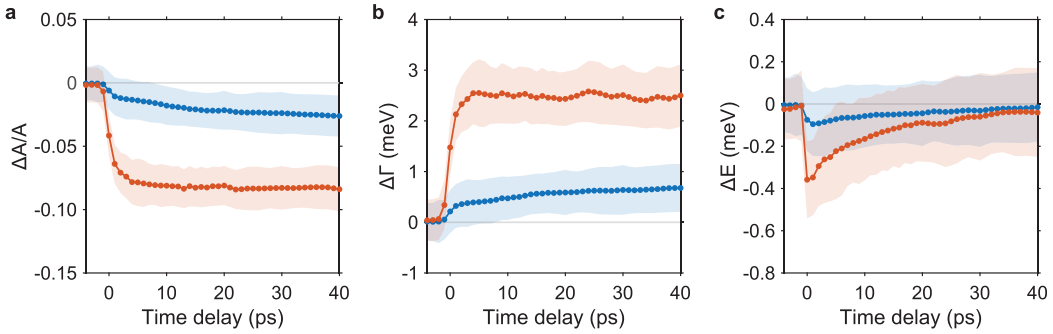

Figure 4. Transient spectral analysis as a function of time delay. Absolute values of (a) pump-induced absorption change $\Delta A/A$, (b) pump-induced line width broadening $\Delta\Gamma$, and (c) pump-induced energy shift ΔE, when the initial $MoSe_2$ exciton densities are $n_m(0) = 4.1 \times 10^{11}$ cm^{-2} (blue) and $n_m(0) = 3.0 \times 10^{12}$ cm^{-2} (orange). Filled circles are the best-fit parameters from the transfer-matrix calculation at each time delay, and shaded regions denote the 90% confidence interval from the fitting.

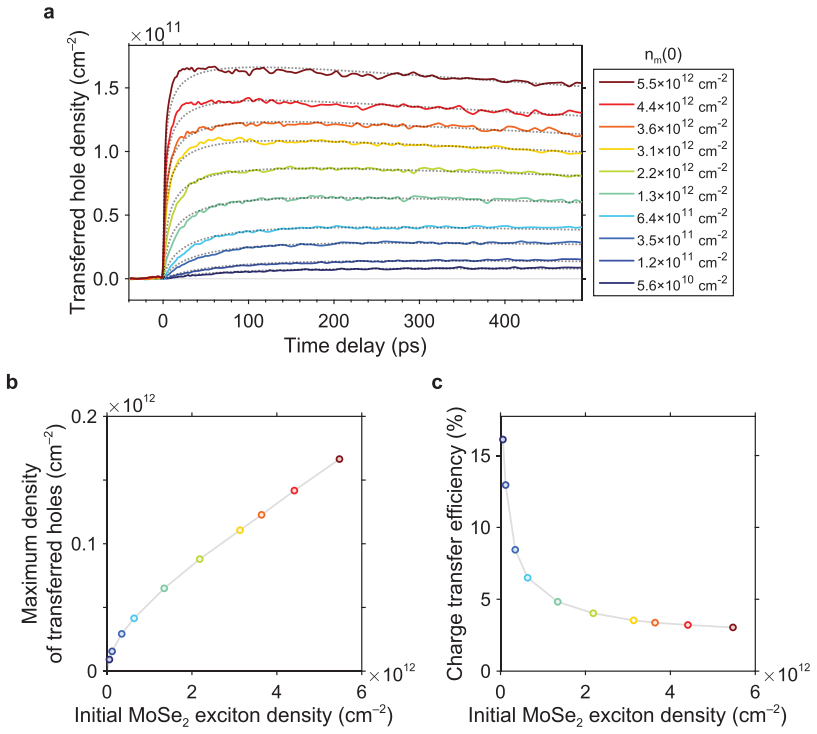

Figure 5. Charge transfer dynamics as a function of the initial $MoSe_2$ exciton density at 100 K. (a) Transferred hole density in the WSe_2 layer is plotted as a function of time delay for different values of the initial $MoSe_2$ exciton density, $n_m(0)$. Black dotted lines are fit results using eqs 1 and 2. (b) The maximum transferred hole density, $\max[n_w(\Delta t)]$, as a function of the initial $MoSe_2$ exciton density, $n_m(0)$. (c) The charge transfer efficiency, defined as $\max[n_w(\Delta t)]/n_m(0)$, as a function of $n_m(0)$.

differential changes, namely, $\Delta R/R = (R_{pump\ on} - R_{pump\ off})/R_{pump\ off}$. In stark contrast to pump-probe spectra measured on similar devices without any hBN spacer,[1] Figure 3a shows that the WSe_2 exciton peak at 1.6923 eV rises slowly and saturates by ~100 ps when the pump fluence is low, which corresponds to the initial $MoSe_2$ exciton density $n_m(\Delta t = 0) = 4.6 \times 10^{11}$ cm^{-2}. When the initial $MoSe_2$ exciton density is increased to $n_m(0) = 2.7 \times 10^{12}$ cm^{-2}, the WSe_2 exciton peak saturates by ~30 ps, as shown in Figure 3b. The observed density-dependent dynamics suggests that nonlinear interactions are involved in the charge transfer process in the $MoSe_2$/hBN/WSe_2 heterostructure. The vertical line cuts of transient reflection spectra at various time delays are shown in Figure 3c,d, which reveal both the saturation of the exciton peak ($\Delta R/R > 0$) and the appearance of a trion peak ($\Delta R/R < 0$).

To quantitatively measure physical properties, we analyzed the reflection contrast spectrum at each time delay and fit it to the transfer-matrix calculation result. We used the Lorentzian oscillator model with complex dielectric constants to approximate the WSe_2 absorption resonance and used the oscillator strength f, central energy E, and line width Γ as fitting parameters at each time delay. Other parameters are fixed to the values obtained from the fitting without the pump (the fit result shown in Figure 1e). The time traces of the extracted quantities are plotted in Figure 4. We calculated $\Delta A/A = (A_{pump\ on} - A_{pump\ off})/A_{pump\ off}$, where A is the absolute value of the absorption, as well as the pump-induced line width broadening $\Delta\Gamma = \Gamma_{pump\ on} - \Gamma_{pump\ off}$ and pump-induced energy shift $\Delta E = E_{pump\ on} - E_{pump\ off}$. Excitation-density-dependent saturation dynamics is observed (Figure 4a), and the line width broadening dynamics follows a similar trend

https://doi.org/10.1021/acs.nanolett.2c04030
Nano Lett. 2022, 22, 10140−10146

(Figure 4b). The absorption saturation and line width broadening effects can be understood as a result of the Pauli blocking at the WSe_2 exciton state by the transferred holes, and these effects are consistent with the repulsive polaron picture.[23] On the other hand, the peak energy slightly red-shifts immediately at $\Delta t = 0$ and then blue-shifts at later time delays. We attribute the initial red-shift to the dielectric screening effect from carriers in the $MoSe_2$ layer; thus, the effect occurs instantaneously after the optical excitation and does not reflect the charge transfer dynamics. After the carrier-induced screening decays, the transferred holes result in the blue-shift of the WSe_2 exciton peak (as well as its saturation and broadening). We emphasize that such spectral analysis and transfer-matrix calculations are crucial to deconvolute various processes from complicated transient reflection spectra and to obtain meaningful results.

From a separate gate-dependent reflection contrast measurement (see Figure S5), we were able to correlate the density of transferred holes in the WSe_2 layer, n_w, and the change of WSe_2 exciton absorption induced by hole doping. This way, we can convert the pump-probe $\Delta A/A$ data (as in Figure 4a) to n_w, which is plotted in Figure 5a as a function of the time delay and excitation density. The estimated density of $MoSe_2$ excitons created by the pump, $n_m(\Delta t = 0)$, ranges from 5.6×10^{10} to 5.5×10^{12} cm^{-2} (see the Supporting Information for details of the calibration). The hole transfer time scale is not only much slower than that without an hBN spacer but also strongly density-dependent. Due to the slower time scale, it competes with several other processes at the picosecond time scale. Most importantly, the exciton−exciton annihilation process within the $MoSe_2$ layer becomes very important at higher pump fluences.[24,25]

The maximum density of transferred holes, $\max[n_w(\Delta t)]$, is plotted in Figure 5b, and the charge transfer efficiency, defined as $\max[n_w(\Delta t)]/n_m(0)$, is plotted in Figure 5c. As the excitation density is increased, there is increased competition between the charge transfer and other nonlinear processes, which leads to a less efficient transfer. This behavior is different from devices without an hBN spacer,[16] where the charge transfer process dominates all other losses and a linear increase of $\max[n_w(\Delta t)]$ is observed as a function of $n_m(0)$ until the transferred hole density becomes too large. In a similar device but with a 3 nm thick hBN spacer, the charge transfer becomes too slow and inefficient, so we were not able to measure any appreciable change of the WSe_2 exciton peak within the measurement window (500 ps).

To quantitatively understand the density-dependent dynamics and competition between different processes, we used coupled rate equations to solve for the exciton and hole densities. The exciton density in the $MoSe_2$ layer is denoted by n_m, while the transferred hole density in the WSe_2 layer is denoted by n_w. The rates of their population change can be expressed as

$$\frac{dn_m}{dt} = -\gamma_m n_m - \frac{1}{2}\gamma_{mm} n_m^2 - \gamma_t n_m \quad (1)$$

$$\frac{dn_w}{dt} = -\gamma_w n_w + \gamma_t n_m + \frac{1}{2}\alpha\gamma_{mm} n_m^2 \quad (2)$$

where γ_m is the $MoSe_2$ exciton population decay rate, γ_w is the WSe_2 hole population decay rate, γ_{mm} is the $MoSe_2$ exciton−exciton annihilation rate, and γ_t is the hole transfer rate from $MoSe_2$ to WSe_2. The last term in eq 2 represents a nonlinear charge transfer mechanism, where the high-energy excitations created by the exciton−exciton annihilation provide additional transfer pathways.

We numerically solved the coupled differential equations with fitting parameters to reproduce the measured density-dependent dynamics and plotted it in Figure 5a as gray dotted lines. The global parameters that give best fits to all excitation densities are $\gamma_m = (100\ ps)^{-1}$, $\gamma_w = (4\ ns)^{-1}$, $\gamma_{mm} = 0.3\ cm^2/s$, and $\gamma_t = (500\ ps)^{-1}$ (see Figure S8 for fit results using different starting parameters). The value of γ_{mm} is consistent with that observed in a previous study with a $MoSe_2$ monolayer,[25] and the intralayer exciton decay rate γ_m represents the effective rate that includes radiative decay, nonradiative decay, and the dynamics between bright and dark excitonic species[26] (see Figure S7 for a separate measurement). Without the nonlinear charge transfer term $\frac{1}{2}\alpha\gamma_{mm}n_m^2$, the very steep saturation at higher excitation densities cannot be reproduced with any reasonable fit parameter values. We estimate that $\alpha = 0.023$, which implies that about 2.3% of the annihilated particles eventually find a way to the WSe_2 layer.

The hole transfer time of 500 ps is over 3 orders of magnitude longer than that observed in a directly contacted $MoSe_2/WSe_2$ heterostructure (<100 fs). The phonon relaxation time to the band edge is negligibly short (optical phonons at ∼40 meV can be emitted efficiently at the femtosecond time scale[27−29]), so the charge transfer process is only slowed down by the increased tunneling barrier and reduced interlayer coupling. However, even though the transfer time scale is much slower, the overall transfer efficiency is still significant, so the optical generation of interlayer excitons is minimally compromised.

The measured efficiency shown in Figure 5c gives additional bounds to the fitting result. In the low-excitation-density limit, the analytical solutions of eqs 1 and 2 show that the transfer efficiency should be $\eta = \gamma_t/(\gamma_t + \gamma_m)$. The measured efficiency of 16% at the lowest excitation density implies that the transfer time τ_t is about 5 times longer than the exciton lifetime τ_m, which is consistent with the measurements and fit results. Note that, without the density-dependent measurements, the lowest-density data alone cannot satisfactorily distinguish the charge transfer time τ_t from other time scales on the same order. In addition, we exclude the possibility of faster charge transfer at higher excitation densities, which would result in higher transfer efficiencies at higher excitation densities. Therefore, we confirm that the charge transfer rate is indeed hundreds of picoseconds in $MoSe_2$/1 nm hBN/WSe_2.

In conclusion, we used a thin hBN spacer between $MoSe_2$ and WSe_2 monolayers to study the effects of the tunneling barrier on the charge transfer time scale and efficiency. We extracted pump-induced saturation, energy shift, and line width broadening at each time delay to distinguish different processes that affect the absorption peak. Density-dependent saturation dynamics reveals competing processes such as exciton−exciton annihilation and nonlinear charge transfer processes. By fitting the solution of coupled rate equations to the measured density-dependent charge transfer dynamics, we found that the intrinsic charge transfer time is ∼500 ps, which is over 3 orders of magnitude slower than without a spacer. Our work opens possibilities of investigating the factors contributing to charge transfer, e.g., the effects of momentum mismatch between the layers, which have not been feasible in directly contacted TMD heterostructures due to the extremely fast

https://doi.org/10.1021/acs.nanolett.2c04030
Nano Lett. 2022, 22, 10140−10146

time scale. Understanding the charge transfer process across various thicknesses of an hBN spacer will allow us to further optimize the generation and control of interlayer excitons with tunable dipole moments and lifetimes.

■ ASSOCIATED CONTENT

Supporting Information

The Supporting Information is available free of charge at https://pubs.acs.org/doi/10.1021/acs.nanolett.2c04030.

Device fabrication methods and characterization results, pump−probe setup and beam profiles for the pump fluence determination, detailed calibration methods for the $MoSe_2$ exciton density using transfer-matrix calculation of absorption, detailed calibration methods for the WSe_2 hole density using gate-dependent absorption measurement, results of coupled rate equations fitting with different conditions (PDF)

■ AUTHOR INFORMATION

Corresponding Author

Yoseob Yoon − *Department of Physics, University of California, Berkeley, California 94720, United States; Materials Sciences Division, Lawrence Berkeley National Laboratory, Berkeley, California 94720, United States;* orcid.org/0000-0002-8832-897X; Email: yoonys@berkeley.edu

Authors

Zuocheng Zhang − *Department of Physics, University of California, Berkeley, California 94720, United States*

Ruishi Qi − *Department of Physics, University of California, Berkeley, California 94720, United States; Materials Sciences Division, Lawrence Berkeley National Laboratory, Berkeley, California 94720, United States*

Andrew Y. Joe − *Department of Physics, University of California, Berkeley, California 94720, United States; Materials Sciences Division, Lawrence Berkeley National Laboratory, Berkeley, California 94720, United States;* orcid.org/0000-0003-4376-7386

Renee Sailus − *School for Engineering of Matter, Transport and Energy, Arizona State University, Tempe, Arizona 85287, United States*

Kenji Watanabe − *Research Center for Functional Materials, National Institute for Materials Science, Tsukuba 305-0044, Japan;* orcid.org/0000-0003-3701-8119

Takashi Taniguchi − *International Center for Materials Nanoarchitectonics, National Institute for Materials Science, Tsukuba 305-0044, Japan;* orcid.org/0000-0002-1467-3105

Sefaattin Tongay − *School for Engineering of Matter, Transport and Energy, Arizona State University, Tempe, Arizona 85287, United States;* orcid.org/0000-0001-8294-984X

Feng Wang − *Department of Physics, University of California, Berkeley, California 94720, United States; Materials Sciences Division, Lawrence Berkeley National Laboratory, Berkeley, California 94720, United States*

Complete contact information is available at: https://pubs.acs.org/10.1021/acs.nanolett.2c04030

Author Contributions

F.W. and Y.Y. conceived the project. Y.Y. performed pump−probe measurements and transfer-matrix calculations. Z.Z., R.Q., and A.Y.J. fabricated the samples and performed gate- and temperature-dependent reflection contrast measurements. K.W. and T.T. grew hBN crystals. R.S. and S.T. grew $MoSe_2$ and WSe_2 crystals. All the authors discussed the results and contributed to the manuscript.

Notes

The authors declare no competing financial interest.

■ ACKNOWLEDGMENTS

This work was primarily supported by the Center for Computational Study of Excited-State Phenomena in Energy Materials (C2SEPEM) at LBNL, funded by the U.S. Department of Energy, Office of Science, Basic Energy Sciences, Materials Sciences and Engineering Division under Contract No. DE-AC02-05CH11231. The device fabrication is supported by the U.S. Department of Energy, Office of Science, Basic Energy Sciences, Materials Sciences and Engineering Division under Contract No. DE-AC02-05CH11231 within the van der Waals heterostructure program (KCWF16). R.S. and S.T. acknowledge primary support from DOE-SC0020653 (materials synthesis), NSF CMMI 1825594 (NMR and TEM studies), NSF DMR-1955889 (purity measurements), NSF CMMI-1933214, NSF 1904716, NSF 1935994, NSF ECCS 2052527, DMR 2111812, and CMMI 2129412 (for defect-structure-quality relations). K.W. and T.T. acknowledge support from the JSPS KAKENHI (Grant Numbers 19H05790 and 20H00354). We thank Y. R. Shen for helpful discussion.

■ REFERENCES

(1) Hong, X.; Kim, J.; Shi, S.-F.; Zhang, Y.; Jin, C.; Sun, Y.; Tongay, S.; Wu, J.; Zhang, Y.; Wang, F. Ultrafast Charge Transfer in Atomically Thin MoS_2/WS_2 Heterostructures. *Nat. Nanotechnol.* **2014**, *9* (9), 682−686.

(2) Jin, C.; Ma, E. Y.; Karni, O.; Regan, E. C.; Wang, F.; Heinz, T. F. Ultrafast Dynamics in van Der Waals Heterostructures. *Nat. Nanotechnol.* **2018**, *13* (11), 994−1003.

(3) Jiang, Y.; Chen, S.; Zheng, W.; Zheng, B.; Pan, A. Interlayer Exciton Formation, Relaxation, and Transport in TMD van Der Waals Heterostructures. *Light Sci. Appl.* **2021**, *10* (1), 72.

(4) Ma, E. Y.; Guzelturk, B.; Li, G.; Cao, L.; Shen, Z.-X.; Lindenberg, A. M.; Heinz, T. F. Recording Interfacial Currents on the Subnanometer Length and Femtosecond Time Scale by Terahertz Emission. *Sci. Adv.* **2019**, *5* (2), No. eaau0073.

(5) Ma, L.; Nguyen, P. X.; Wang, Z.; Zeng, Y.; Watanabe, K.; Taniguchi, T.; MacDonald, A. H.; Mak, K. F.; Shan, J. Strongly Correlated Excitonic Insulator in Atomic Double Layers. *Nature* **2021**, *598* (7882), 585−589.

(6) Choi, J.; Florian, M.; Steinhoff, A.; Erben, D.; Tran, K.; Kim, D. S.; Sun, L.; Quan, J.; Claassen, R.; Majumder, S.; Hollingsworth, J. A.; Taniguchi, T.; Watanabe, K.; Ueno, K.; Singh, A.; Moody, G.; Jahnke, F.; Li, X. Twist Angle-Dependent Interlayer Exciton Lifetimes in van Der Waals Heterostructures. *Phys. Rev. Lett.* **2021**, *126* (4), 047401.

(7) Barré, E.; Karni, O.; Liu, E.; O'Beirne, A. L.; Chen, X.; Ribeiro, H. B.; Yu, L.; Kim, B.; Watanabe, K.; Taniguchi, T.; Barmak, K.; Lui, C. H.; Refaely-Abramson, S.; da Jornada, F. H.; Heinz, T. F. Optical Absorption of Interlayer Excitons in Transition-Metal Dichalcogenide Heterostructures. *Science* **2022**, *376* (6591), 406−410.

(8) Kim, J.; Jin, C.; Chen, B.; Cai, H.; Zhao, T.; Lee, P.; Kahn, S.; Watanabe, K.; Taniguchi, T.; Tongay, S.; Crommie, M. F.; Wang, F. Observation of Ultralong Valley Lifetime in WSe_2/MoS_2 Heterostructures. *Sci. Adv.* **2017**, *3* (7), e1700518.

(9) Rivera, P.; Schaibley, J. R.; Jones, A. M.; Ross, J. S.; Wu, S.; Aivazian, G.; Klement, P.; Seyler, K.; Clark, G.; Ghimire, N. J.; Yan, J.; Mandrus, D. G.; Yao, W.; Xu, X. Observation of Long-Lived Interlayer Excitons in Monolayer $MoSe_2$-WSe_2 Heterostructures. *Nat. Commun.* **2015**, *6* (1), 6242.
(10) Zhang, Z.; Regan, E. C.; Wang, D.; Zhao, W.; Wang, S.; Sayyad, M.; Yumigeta, K.; Watanabe, K.; Taniguchi, T.; Tongay, S.; Crommie, M.; Zettl, A.; Zaletel, M. P.; Wang, F. Correlated Interlayer Exciton Insulator in Heterostructures of Monolayer WSe_2 and Moiré WS_2/WSe_2. *Nat. Phys.* **2022**, *18* (10), 1214−1220.
(11) Gu, J.; Ma, L.; Liu, S.; Watanabe, K.; Taniguchi, T.; Hone, J. C.; Shan, J.; Mak, K. F. Dipolar Excitonic Insulator in a Moiré Lattice. *Nat. Phys.* **2022**, *18* (4), 395−400.
(12) Wang, Z.; Rhodes, D. A.; Watanabe, K.; Taniguchi, T.; Hone, J. C.; Shan, J.; Mak, K. F. Evidence of High-Temperature Exciton Condensation in Two-Dimensional Atomic Double Layers. *Nature* **2019**, *574* (7776), 76−80.
(13) Wu, F.-C.; Xue, F.; MacDonald, A. H. Theory of Two-Dimensional Spatially Indirect Equilibrium Exciton Condensates. *Phys. Rev. B* **2015**, *92* (16), 165121.
(14) Togan, E.; Lim, H.-T.; Faelt, S.; Wegscheider, W.; Imamoglu, A. Enhanced Interactions between Dipolar Polaritons. *Phys. Rev. Lett.* **2018**, *121* (22), 227402.
(15) Lagoin, C.; Bhattacharya, U.; Grass, T.; Chhajlany, R. W.; Salamon, T.; Baldwin, K.; Pfeiffer, L.; Lewenstein, M.; Holzmann, M.; Dubin, F. Extended Bose-Hubbard Model with Dipolar Excitons. *Nature* **2022**, *609* (7927), 485−489.
(16) Ceballos, F.; Bellus, M. Z.; Chiu, H.-Y.; Zhao, H. Probing Charge Transfer Excitons in a $MoSe_2$-WS_2 van Der Waals Heterostructure. *Nanoscale* **2015**, *7* (41), 17523−17528.
(17) Schaibley, J. R.; Rivera, P.; Yu, H.; Seyler, K. L.; Yan, J.; Mandrus, D. G.; Taniguchi, T.; Watanabe, K.; Yao, W.; Xu, X. Directional Interlayer Spin-Valley Transfer in Two-Dimensional Heterostructures. *Nat. Commun.* **2016**, *7* (1), 13747.
(18) Ji, Z.; Hong, H.; Zhang, J.; Zhang, Q.; Huang, W.; Cao, T.; Qiao, R.; Liu, C.; Liang, J.; Jin, C.; Jiao, L.; Shi, K.; Meng, S.; Liu, K. Robust Stacking-Independent Ultrafast Charge Transfer in MoS_2/WS_2 Bilayers. *ACS Nano* **2017**, *11* (12), 12020−12026.
(19) Zhu, H.; Wang, J.; Gong, Z.; Kim, Y. D.; Hone, J.; Zhu, X.-Y. Interfacial Charge Transfer Circumventing Momentum Mismatch at Two-Dimensional van Der Waals Heterojunctions. *Nano Lett.* **2017**, *17* (6), 3591−3598.
(20) Zheng, S.-W.; Wang, H.-Y.; Wang, L.; Wang, H.; Sun, H.-B. Layer-Dependent Electron Transfer and Recombination Processes in MoS_2/WSe_2 Multilayer Heterostructures. *J. Phys. Chem. Lett.* **2020**, *11* (22), 9649−9655.
(21) Wang, Z.; Altmann, P.; Gadermaier, C.; Yang, Y.; Li, W.; Ghirardini, L.; Trovatello, C.; Finazzi, M.; Duò, L.; Celebrano, M.; Long, R.; Akinwande, D.; Prezhdo, O. V.; Cerullo, G.; Dal Conte, S. Phonon-Mediated Interlayer Charge Separation and Recombination in a $MoSe_2$/WSe_2 Heterostructure. *Nano Lett.* **2021**, *21* (5), 2165−2173.
(22) Zimmermann, J. E.; Axt, M.; Mooshammer, F.; Nagler, P.; Schüller, C.; Korn, T.; Höfer, U.; Mette, G. Ultrafast Charge-Transfer Dynamics in Twisted MoS_2/WSe_2 Heterostructures. *ACS Nano* **2021**, *15* (9), 14725−14731.
(23) Sidler, M.; Back, P.; Cotlet, O.; Srivastava, A.; Fink, T.; Kroner, M.; Demler, E.; Imamoglu, A. Fermi Polaron-Polaritons in Charge-Tunable Atomically Thin Semiconductors. *Nat. Phys.* **2017**, *13* (3), 255−261.
(24) Sun, D.; Rao, Y.; Reider, G. A.; Chen, G.; You, Y.; Brézin, L.; Harutyunyan, A. R.; Heinz, T. F. Observation of Rapid Exciton-Exciton Annihilation in Monolayer Molybdenum Disulfide. *Nano Lett.* **2014**, *14* (10), 5625−5629.
(25) Kumar, N.; Cui, Q.; Ceballos, F.; He, D.; Wang, Y.; Zhao, H. Exciton-Exciton Annihilation in $MoSe_2$ Monolayers. *Phys. Rev. B* **2014**, *89* (12), 125427.
(26) Robert, C.; Lagarde, D.; Cadiz, F.; Wang, G.; Lassagne, B.; Amand, T.; Balocchi, A.; Renucci, P.; Tongay, S.; Urbaszek, B.; Marie, X. Exciton Radiative Lifetime in Transition Metal Dichalcogenide Monolayers. *Phys. Rev. B* **2016**, *93* (20), 205423.
(27) Mahrouche, F.; Rezouali, K.; Mahtout, S.; Zaabar, F.; Molina-Sánchez, A. Phonons in WSe_2/$MoSe_2$ van Der Waals Heterobilayers. *Phys. Status Solidi B* **2022**, *259* (1), 2100321.
(28) Trovatello, C.; Katsch, F.; Borys, N. J.; Selig, M.; Yao, K.; Borrego-Varillas, R.; Scotognella, F.; Kriegel, I.; Yan, A.; Zettl, A.; Schuck, P. J.; Knorr, A.; Cerullo, G.; Conte, S. D. The Ultrafast Onset of Exciton Formation in 2D Semiconductors. *Nat. Commun.* **2020**, *11* (1), 5277.
(29) Madéo, J.; Man, M. K. L.; Sahoo, C.; Campbell, M.; Pareek, V.; Wong, E. L.; Al-Mahboob, A.; Chan, N. S.; Karmakar, A.; Mariserla, B. M. K.; Li, X.; Heinz, T. F.; Cao, T.; Dani, K. M. Directly Visualizing the Momentum-Forbidden Dark Excitons and Their Dynamics in Atomically Thin Semiconductors. *Science* **2020**, *370* (6521), 1199−1204.

https://doi.org/10.1021/acs.nanolett.2c04030
Nano Lett. 2022, 22, 10140−10146